

# Comprehensive computational model of single- and dual-loop optoelectronic oscillators with experimental verification

Etgar C. Levy,<sup>1,\*</sup> Olukayode Okusaga,<sup>3</sup> Moshe Horowitz,<sup>1</sup> Curtis R. Menyuk,<sup>2</sup> Weimin Zhou,<sup>3</sup> and Gary M. Carter<sup>2</sup>

<sup>1</sup>*Department of Electrical Engineering, Technion - Israel Institute of Technology, Haifa 32000 Israel*

<sup>2</sup>*Department of Electrical Engineering, University of Maryland, Baltimore, Maryland 21250 USA*

<sup>3</sup>*U.S. Army Research Laboratory, Adelphi, Maryland USA*  
[\\*etgarlevy@gmail.com](mailto:etgarlevy@gmail.com)

**Abstract:** We describe a comprehensive computational model for single-loop and dual-loop optoelectronic oscillators (OEOs). The model takes into account the dynamical effects and noise sources that are required to accurately model OEOs. By comparing the computational and experimental results in a single-loop OEO, we determined the amplitudes of the white noise and flicker noise sources. We found that the flicker noise source contains a strong component that linearly depends on the loop length. Therefore, the flicker noise limits the performance of long-cavity OEOs ( $\gtrsim 5$  km) at low frequencies ( $f < 500$  Hz). The model for a single-loop OEO was extended to model the dual-loop injection-locked OEO (DIL-OEO). The model gives the phase-noise, the spur level, and the locking range of each of the coupled loops in the OEO. An excellent agreement between theory and experiment is obtained for the DIL-OEO. Due to its generality and accuracy, the model is important for both designing OEOs and studying the physical effects that limit their performance. We demonstrate theoretically that it is possible to reduce the first spur in the DIL-OEO by more than 20 dB relative to its original performance by changing its parameters. This theoretical result has been experimentally verified.

© 2010 Optical Society of America

**OCIS codes:** (060.2320) Fiber optics amplifiers and oscillators; (230.0250) Optoelectronics; (230.4910) Oscillators.

---

## References and links

1. X. S. Yao and L. Maleki, "Optoelectronic microwave oscillator," *J. Opt. Soc. Am. A* **13**, 1725–1735 (1996).
2. W. Zhou and G. Blasche, "Injection-locked dual opto-electronic oscillator with ultra-low phase noise and ultra-low spurious level," *IEEE Trans. Microwave Theory Tech.* **53**, 929–933 (2005).
3. D. Dahan, E. Shumakher, and G. Eisenstein, "Self-starting ultralow-jitter pulse source based on coupled optoelectronic oscillators with an intracavity fiber parametric amplifier," *Opt. Lett.* **30**, 1623–1625 (2005).
4. C. R. Menyuk, E. C. Levy, O. Okusaga, G. M. Carter, M. Horowitz, and W. Zhou "An analytical model of the dual-injection-locked opto-electronic oscillator," *IFCS* (2009).
5. Y. K. Chembo, L. Larger, H. Tavernier, R. Bendoula, E. Rubiola and P. Colet, "Dynamic instabilities of microwaves generated with optoelectronic oscillators," *Opt. Lett.* **32**, 2571–2573 (2007).

6. E. C. Levy, M. Horowitz, and C. R. Menyuk, "Modeling opto-electronic oscillators," *J. Opt. Soc. Am. B* **26**, 148–159 (2009).
  7. O. Okusaga, W. Zhou, E. C. Levy, M. Horowitz, G. M. Carter, and C. R. Menyuk, "Experimental and simulation study of dual injection-locked OEOs," *IFCS* (2009).
  8. O. Okusaga, E. J. Adles, E. C. Levy, M. Horowitz, G. M. Carter, C. R. Menyuk, and W. Zhou, "Spurious mode suppression in dual injection-locked optoelectronic oscillators," *IFCS* (2010).
  9. E. C. Levy, O. Okusaga, M. Horowitz, C. R. Menyuk, W. Zhou, and G. M. Carter, "Study of dual-loop optoelectronic oscillators," *IFCS* (2009).
  10. E. Rubiola, E. Salik, S. Huang, N. Yu, and L. Maleki, "Photonic-delay technique for phase-noise measurement of microwave oscillators," *J. Opt. Soc. Am. B* **22**, 987–997 (2005).
  11. N. J. Kasdin, "Discrete simulation of colored noise and stochastic processes and  $1/f^\alpha$  power law noise generation," *IEEE Proc.* **83**, 802–827 (1995).
- 

## 1. Introduction

Optoelectronic oscillators (OEOs), first introduced by Yao and Maleki in 1996 [1], are used to generate signals in X-band with a low phase noise. These hybrid opto-electronic devices contain a long optical fiber, typically in the range of 4–6 km. The RF signal is modulated onto an optical carrier at the entry to the fiber, which is then demodulated at the exit. Thus, the OEO is effectively a high- $Q$  RF cavity. Such a high- $Q$  cavity makes possible the generation of a high-frequency signal whose phase noise is nearly independent of the oscillation frequency. Furthermore, the use of a long optical fiber and a tunable narrowband RF filter makes it possible to tune the oscillating signal over a very broad frequency range. These important advantages make the OEO an attractive candidate to replace classical oscillators such as multiplied quartz crystals or phase-locked dielectric resonator oscillators.

Due to the length of the optical fiber, the cavity mode spacing is too small to filter out a single cavity mode using an RF filter. Therefore, the RF spectrum of single-loop OEOs contains strong spurs at the cavity mode frequencies. OEOs with two or more coupled cavities have been used to reduce the spurs [2, 3]. In the work of Zhou *et al.* [2], a long loop OEO, called the master loop, generates an RF signal with a low phase noise. The spurs of the master loop are significantly attenuated by injection-locking the master loop to another short-loop OEO, called the slave loop. The OEO has several parameters that can be varied over a wide range, and determining the performance at frequencies close-in to the carrier with even one set of parameters is time-consuming. As a consequence, it is not possible to comprehensively explore the parameter space experimentally; so it is essential to develop a comprehensive model that is capable of accurately exploring the OEO performance as a function of the OEO parameters.

Several models have been presented for studying the phase noise in OEOs. Yao and Maleki have presented an analytical expression for the phase noise in a single-loop OEO [1] using a model that assumes that the signal's change per round-trip at any point in the loop is small and treats all the loop elements as distributed, rather than lumped. The Yao-Maleki model gives the dependence of the time-averaged phase noise on the frequency offset from the carrier frequency, the cavity length, the oscillation power, and the amplitude of the white noise source. In [4] we introduced a reduced model for calculating the phase noise in a dual-injection-locked OEO (DIL-OEO) that is based on the Yao and Maleki model, and like that model assumes that the signal's change per round-trip at any point in both loops is small. Chembo *et al.* [5] developed a model for a single-loop OEO that is based on a delay-differential equation for studying the signal dynamics in single-loop OEOs. This model assumes that the signal variation along the cavity is small, so that the order of the components does not affect the round-trip signal transmission. In previous work, we have developed a comprehensive model to study a single-loop OEO [6]. This model generalized the Yao-Maleki model and includes all of the physical effects in the Yao-Maleki model as well as other physical effects that are needed to calculate important features of the OEO dynamics, such as the fast response time of the modulator, the ability of

the OEO to oscillate in several cavity modes, and amplitude fluctuations that are induced by the input noise.

In this manuscript, we describe a computational model for single- and dual-injection-locked OEOs (DIL-OEOs) that is a significant extension of the model that is described in Ref. [6], which only applied to a single-loop OEO. This extended model has been experimentally verified [7, 8]. In order to obtain agreement between theory and experiment, we added to the model described in Ref. [6] a phase flicker ( $1/f$ ) noise source, gain saturation in the RF amplifiers, and the spectrum of the RF filter. By extracting the magnitude of the phase flicker noise amplitude from phase measurements in single-loop OEOs with different cavity lengths, we have found that the phase flicker noise contains a strong component with an amplitude that depends on the square-root of cavity length. Therefore, in long-cavity OEOs ( $L > 5$  km) the phase noise at low frequencies ( $f < 500$  Hz) is dominated by the phase flicker noise. A good quantitative agreement between theory and experiments is obtained for the phase noise spectrum and the spur levels of both the slave and the master loops in the DIL-OEO. In contrast to the reduced model that we previously described in [4], this model takes into account the full OEO dynamics, including the growth of the oscillator signal from noise, rather than assuming steady-state operation. Thus, unlike the model in [4], it is capable of determining the locking bandwidth of the two loops in the DIL-OEO. Moreover, this model takes into account the locations of the lumped elements in each loop, rather than treating them as distributed elements. As a consequence, this model can accurately describe the effect of large lumped coupling between the loops of the DIL-OEO, as well as gain, loss, and gain saturation. Since this computational model is based on the full physics, it is inherently more trustworthy than the reduced models. As is almost the case when comparing simplified or reduced models to more complete or full models, there is a tradeoff between computational speed and accuracy. Our view is that for modeling OEOs, this tradeoff favors the use of the full model. It runs quickly — taking less than two minutes of CPU time on a standard desktop computer for one set of parameters — and has allowed us to examine a broad parameter range.

We used our model to theoretically study how to improve the DIL-OEO performance. Our model predicted that it is possible to reduce the magnitude of the first spur that is obtained in the master loop of the DIL-OEO by 20 dB relative to the level in the original experiments [7]. The decrease in the spur level is obtained by increasing the slave loop length by a factor of 10 and by using a strong injected signal with a power of  $-6$  dB with respect to the oscillating signal in both loops. The increase in the slave loop length and the increase in the power injection ratio contribute about 10 dB each to the decrease in the spur level. Subsequently performed experiments verified our model predictions, and guided by the theoretical results we were able to significantly reduce the spur level. These experiments have been presented in part in [8] and will be presented in full elsewhere.

The remainder of this paper is organized as follows. In Sec. 2 we review the single-loop OEO model, including the generation of the flicker noise, and we present the model for DIL-OEO. In Sec. 3 we present comparison between the experimental results and the theoretical results for the phase noise in a single-loop OEO and DIL-OEO. A good agreement is achieved between theory and experiment. In Sec. 4, we present a theoretical study of methods to reduce the spur level. The theoretical calculations that were subsequently verified experimentally show that a significant reduction in the spur level can be achieved by increasing the loop delay of the slave loop and optimizing the coupling between the loops. Finally, we summarize our results and conclude in Sec. 5.

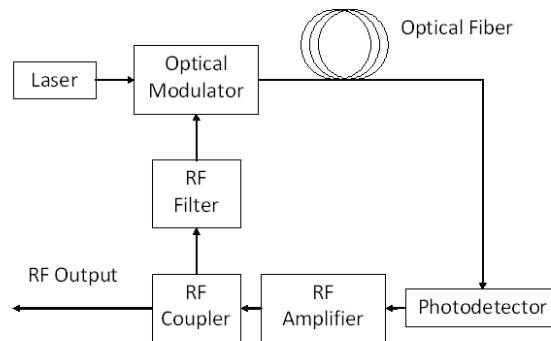


Fig. 1. Schematic illustration of the single-loop OEO configuration

## 2. Model description

In this section we describe our model for the single-loop and dual-loop OEO configurations. As previously noted in [6], four different time/frequency scales play a role in the OEO. At the highest frequency scale, we have the optical carrier in the optical fiber, which is close to 200 THz. However, the role of the optical carrier is completely passive. The light merely serves to carry the RF signal from one end of the optical fiber to the other and has no effect on the OEO dynamics. We therefore model the optical fiber as a fixed delay of the RF signal and ignore the dynamics on the optical frequency scale. At the next-highest frequency scale, we have the RF carrier at around 10 GHz. At this scale, the RF filters in the OEO loops, which typically have a bandwidth of about 10 MHz, filter out harmonics of the RF signal that appear due to gain saturation in the RF amplifiers and optical modulators. At the next-highest frequency scale, we have the inverse of the round-trip time in the OEO loops. This time may be as short as  $0.2 \mu\text{s}$  for a 40 m loop, corresponding to a frequency of 5 MHz, and may be as long as  $30 \mu\text{s}$  for a 6 km loop, corresponding to 33 kHz. Finally, we have the frequency scale of the phase noise. We are interested in the frequency range from about 1 Hz to 100 kHz. A point that should be emphasized is that the last two scales are not well-separated. In most previous models [1, 4, 5], the behavior during one round-trip in an OEO loop was not resolved. As a consequence, these previous models are simpler than ours and use less CPU time than ours does; however, they also cannot reliably achieve the quantitative agreement with experiment that our model does.

By contrast, it is not necessary to resolve phenomena that occur on the time scale of the 100 ps oscillation period of the RF carrier, since this time scale is widely separated from the two longer time scales.

In a typical simulation of the DIL-OEO, we calculate the signal evolution for 0.01 seconds, corresponding to 50,000 round-trips in a short slave loop with a 40 m loop. This simulation takes approximately 2 minutes on an IBM with a CPU speed of 2.33 GHz and 4 GB of RAM.

### 2.1. Modeling the oscillating signal and its noise in a single-loop OEO

In this sub-section, we review the single-loop OEO model; more details may be found in [6]. A schematic illustration of the single-loop OEO is given in Fig. 1. Light from a laser is fed into an electro-optic modulator, which is used to convert microwave oscillations into a modulation of the light intensity. The modulated light is sent through a long optical fiber and is then detected using a photodetector, which converts the modulated light signal into an electrical signal. The electrical signal is then amplified, filtered, and fed back into the electrical port of the modulator.

In the analysis of a single-loop OEO, it is assumed that due to the narrow bandwidth of the OEO filter, the voltage applied to the modulator,  $V_{\text{in}}(t)$ , is approximately a sinusoidal wave with an angular carrier frequency  $\omega_c = 2\pi f_c$ , a time-dependent phase  $\phi(t)$ , and a time-dependent amplitude  $|a_{\text{in}}^{\text{mod}}(t)|$ , so that

$$V_{\text{in}}(t) = |a_{\text{in}}^{\text{mod}}(t)| \cos[\omega_c t - \phi(t)] = \frac{1}{2} a_{\text{in}}^{\text{mod}}(t) \exp(-i\omega_c t) + \text{c.c.}, \quad (1)$$

where  $a_{\text{in}}^{\text{mod}}(t) = |a_{\text{in}}^{\text{mod}}(t)| \exp[i\phi(t)]$  is the complex envelope or the phasor of the voltage  $V_{\text{in}}(t)$ . Since the OEO signal is narrow-band we assume that  $|d\phi/dt| \ll \omega_c$  and  $d|a_{\text{in}}^{\text{mod}}|/dt \ll |a_{\text{in}}^{\text{mod}}|\omega_c$ . The phasor of the oscillating signal contains all the information in both the amplitude and phase noise spectrum. As noted previously, the nonlinear response of the OEO components such as the electro-optic modulator and the RF amplifiers creates high-harmonic components that are centered around angular frequencies  $m\omega_c$  with  $m > 1$ , where  $m$  is an integer, but these higher harmonics are filtered out, so that it is sufficient to model only the propagation of the phasor that represents the signal around the angular carrier frequency  $\omega_c$ . The evolution of the phasor  $a_{\text{in}}^{\text{mod}}(t)$  in the OEO cavity is calculated by taking into account the effect of all the OEO components: the electro-optic modulator, the fiber delay, the photodetector, the RF amplifiers with saturation, and the RF filter.

The electro-optic modulator that is analyzed in our model is a Mach-Zehnder modulator. We used the Jacobi-Anger expansion to calculate the first harmonic in the nonlinear modulator response [1, 6]. Keeping only the first harmonic term, the phasor at the output of the photodetector,  $a_{\text{out}}^{\text{PD}}$ , is related to the phasor at the input RF port of the modulator,  $a_{\text{in}}^{\text{mod}}$ , by

$$a_{\text{out}}^{\text{PD}}(T) = -\alpha P_0 \eta \rho R \cos(\pi V_B / V_{\pi, \text{DC}}) J_1 \left( \pi \left| a_{\text{in}}^{\text{mod}}(T) \right| / V_{\pi, \text{AC}} \right) \exp[i\phi(T)]. \quad (2)$$

where  $\alpha$  is the insertion loss in the modulator and the detector,  $P_0$  is the optical power at the modulator input,  $\eta$  is a parameter determined by the extinction ratio of the modulator  $(1 + \eta)/(1 - \eta)$ ,  $\rho$  is the responsivity of the photodetector,  $R$  is the impedance at the output of the detector,  $V_{\pi, \text{DC}}$  and  $V_{\pi, \text{AC}}$  are the modulator half-wave voltages for the DC and AC voltages, respectively, and  $V_B$  is the DC bias voltage.

Our experimental setup [7] included three identical RF amplifiers, each with a small-signal gain of 20 dB. The gain saturation of the three cascaded RF amplifiers was measured and then used in the model. The gain saturation curve is shown in Fig. 2(a); it describes the relation between output power of the 3 RF amplifiers  $P_{\text{out}} = |a_{\text{out}}^{\text{amp}}(t)|^2 / 2R$  and the input power  $P_{\text{in}} = |a_{\text{in}}^{\text{amp}}(t)|^2 / 2R$ , where  $a_{\text{in}}^{\text{amp}}(t) = a_{\text{out}}^{\text{PD}}(t)$ .

The model also takes into account the RF filter response and its dynamic effects. The dynamic effects are taken into account by using the time history of the phasor, which is chosen to be longer than the response time of the filter. The filter implementation and its associated dynamic effects are described in detail in [6]. The full width at half maximum (FWHM) of the RF filter bandwidth that is used in our experimental setup [7] was equal to  $\Omega_F = 8$  MHz. In our model, we used the experimentally measured transmission function that is shown in Fig. 2(b). To ensure that the RF filter has a casual response, a linear phase chirp was added to the measured transmission function that corresponds to a delay of 0.1  $\mu\text{s}$ .

We have implemented our model by discretizing the phasor of the oscillating signal along the loop using an array containing  $N$  points, which implies a time separation or resolution time  $\delta t = \tau/N$ . The number of points was chosen so that the simulation bandwidth  $\Delta f = 1/\delta t$  is broader than the RF filter FWHM bandwidth,  $\Omega_F$ . Furthermore, we checked that the results did not change when we increased the number of points  $N$ .

Additive white Gaussian noise is included in the model and is added to the phasor of the oscillating signal. Additive white Gaussian noise is added at the output of the photodetector and at the input of each of the RF amplifiers at each round trip. The spectral power density of the additive noise at the output of the photodetector and at the input of the RF amplifiers is determined by evaluating the shot noise power density,  $\rho_{\text{SN}}$ , and the thermal noise power density,  $\rho_{\text{th}}$ , respectively. The photodetector's shot noise power density is evaluated using the formula:  $\rho_{\text{SN}} = 2eI_{\text{PD}}R$ , where  $I_{\text{PD}} = \langle |a_{\text{out}}^{\text{PD}}(t)| \rangle_{\tau}/R$  is the photodetector's current, averaged over one round trip, and  $\langle \rangle_{\tau}$  denotes averaging over the round-trip time. The spectral power density of the thermal noise, given by  $\rho_{\text{th}} = (\text{NF})k_{\text{B}}T$ , is determined by the noise factor NF of the RF amplifiers. The noise factor was determined empirically, and in order to obtain the best match between theory and experiment we typically used a noise factor of  $\text{NF} = 4$ . We added noise to the oscillating phasor in the same manner that is described in [6]. During each round trip, we added  $N$  mutually independent noise variables  $w_i$ ,  $i = 1, \dots, N$ , to the array of the oscillating phasor, such that the variance of the noise variables is set by the relation  $\langle |w_i|^2 \rangle_{\tau}/2R = \rho/\tau$ , where  $\rho$  is the noise power density. A complex Gaussian distribution is assumed, and each of the real and imaginary parts of the noise variables is normally distributed with a variance  $\rho R/\tau$ . The noise is added in the simulation after the photodetector and before each of the RF amplifiers with a noise power density of  $\rho_{\text{SN}}$  and  $\rho_{\text{th}}$ , respectively. We note that the main contribution of the thermal noise to the phase noise is from the noise that is added at the input of the first RF amplifier. As a result, the phase noise in our simulation is practically determined by the total white noise that is added between the photodetector and the first RF amplifier, which has a noise power density of  $\rho_{\text{total}} = \rho_{\text{th}} + \rho_{\text{SN}}$ .

The experimental results indicate that phase flicker noise ( $1/f$ ) is the dominant noise source at low frequencies ( $f < 500$  Hz) of long-cavity OEOs ( $L \simeq 5$  km). Therefore, we include in our model a phase flicker noise source. In electronic devices, such as RF amplifiers, flicker noise is generated at DC and then nonlinearly upconverted to the carrier frequency [10]. The same appears to be true in the optical domain where some combinations of fiber dispersion and nonlinearity, double-scattering processes, and environmental effects can convert electronic flicker noise to optical flicker noise and other odd powers of the frequency in the phase noise

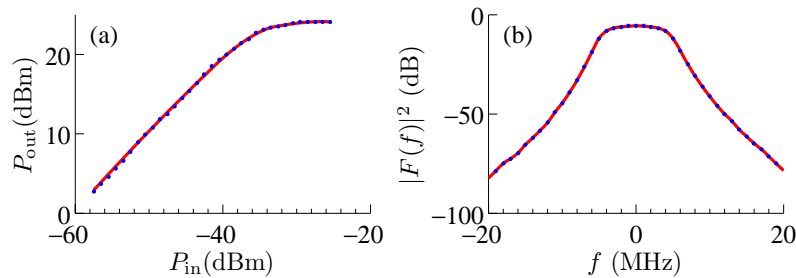


Fig. 2. (a) The measured electrical power at the output of the 3 RF amplifiers as a function of the input power. (b) The measured spectrum of the RF filter as measured experimentally and used in the model.

spectrum. Thus, the phase flicker noise is multiplicative. We model the phase flicker noise by multiplying the phasor of the oscillating signal by  $\exp[i\theta(t)]$  at the output of the RF amplifiers, where  $\theta(t)$  is a time-domain realization of flicker ( $1/f$ ) noise, which has a power spectral density  $\langle S_\theta(f) \rangle = b_{-1}/f$  rad<sup>2</sup>/Hz. We found that the effect of the phase noise was independent of the location in the loop where we added the flicker noise. The flicker coefficient  $b_{-1}$  is dimensionless, and it determines the power spectral density of the phase flicker noise. The flicker coefficient was determined empirically in order to obtain the best match between theory and experiment, and in a short-loop-length OEO we used a flicker coefficient of  $1 - 2 \times 10^{-12}$ , which is a typical range for RF amplifiers [10]. Flicker noise is correlated, and it can be modeled by linearly filtering white Gaussian noise. Several different techniques exist. We used the approach that is described in Ref. [11]. In sub-section 2.2, we describe in detail how the flicker noise was generated in our model.

During each round trip, we calculated the evolution of the phasor, taking into account the additive white noise and the multiplicative flicker noise. It is necessary to record the phasor  $a_{\text{in}}^{\text{mod}}(t)$  over some large number  $N_{\text{RT}}$  round trips in order to calculate the phase noise power spectral density at low frequencies. The phase noise of the oscillating signal is calculated using the Fourier transform of the accumulated phasor [6]. The lowest frequency that can be resolved is on the order of  $1/T_{\text{tot}}$  where  $T_{\text{tot}} = N_{\text{RT}}\tau$  is the overall accumulation time of the phasor in the simulation run. The power spectral density of the phase noise is then calculated by averaging the power spectral density that we obtain from individual simulation runs over  $N_{\text{avg}}$  realizations. In our simulations, we used a range of accumulation times  $T_{\text{tot}} = 10 - 100$  ms, a range of resolution times  $\delta t = 50 - 60$  ns, and a range of numbers of realizations  $N_{\text{avg}} = 20 - 100$ . We checked the convergence of our computational results by verifying that the power spectral density of the phase noise did not change when we increased the resolution time  $\delta t$  or the number of realizations  $N_{\text{avg}}$ .

## 2.2. Modeling the flicker noise

In our simulation model, we used the approach that is described in Ref. [11] to create a discrete time series,  $\theta_k$ ,  $k = 1, \dots, M$ , with an averaged spectrum of  $\langle S_\theta(f) \rangle = b_{-1}/f$ . The length of the time series is determined by the ratio between the total accumulation time and the resolution time of the simulation,  $M = T_{\text{tot}}/\delta t = N_{\text{RT}}N$ . We started with discrete white Gaussian noise in the time domain,  $w_k$ . The variance of the white noise was set so that  $\langle w_k \rangle^2 = 2\pi b_{-1}$ . The filtering in the simulation was implemented in the frequency domain, so that

$$\Theta(v_n) = H(v_n)W(v_n), \quad (3)$$

where  $n = 1, \dots, M$ ,  $v_n = -1/2 + (n-1)/M$  is the normalized fourier frequency,  $\Theta(v_n)$  is the filtered noise,  $H(v_n)$  is the filter response in the frequency domain given by

$$\begin{aligned} H(v_n) &= [1 - \exp(-2\pi i v_n)]^{-1/2}, \\ H(v_{M/2+1}) &= 0, \end{aligned} \quad (4)$$

and  $W(v_n)$  is the discrete Fourier transform of  $w_k$  defined by

$$W(v_n) = \sum_{k=1}^M w_k \exp[2\pi i(k-1)(n-1)/M]. \quad (5)$$

The discrete time series of the flicker noise in the time domain is given by applying an inverse Fourier transform to the filtered noise  $\Theta(v_n)$

$$\theta_k = (1/M) \sum_{n=1}^M \Theta(v_n) \exp[-2\pi i(k-1)(n-1)/M]. \quad (6)$$

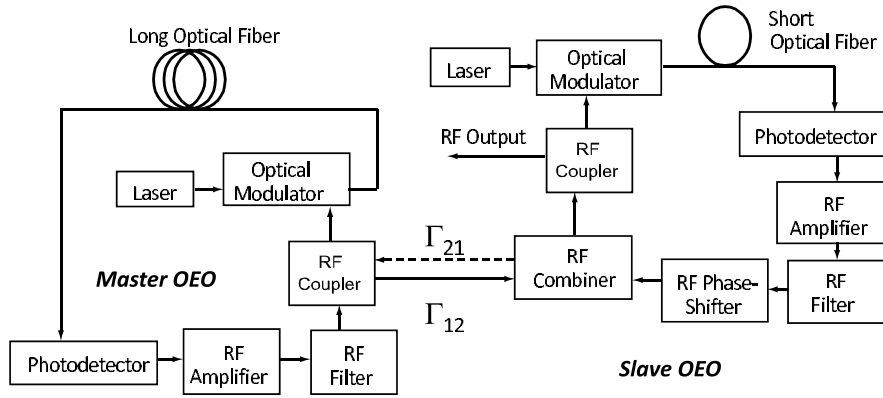


Fig. 3. Schematic description of the DIL-OEO. The DIL-OEO operates in a master-slave configuration. The longer loop, referred to as the master loop, generates a harmonic signal with a very low phase noise. The shorter loop, referred to as the slave loop, is used to decrease the amplitude of the spurs. Part of the master signal,  $\Gamma_{12}$ , is injected into the slave loop, as indicated schematically by the solid arrow. The dashed arrow indicates that part of the slave signal,  $\Gamma_{21}$ , is coupled back into the master loop.

The discrete time series  $\theta_k$  has an averaged spectrum of  $\langle S_\theta(f) \rangle = b_{-1}/f$ . The series  $\theta_k$  is generated at the beginning of each simulation run. During each round trip, we use  $N$  subsequent terms of the series to multiply the array of the phasor by  $\exp(i\theta_k)$ , so that by the end of the run all the terms of the series are used only once.

### 2.3. Modeling dual-loop OEOs

Figure 3 shows a schematic description of the DIL-OEO configuration. The lumped components in the loop, as well as the added noise, are modeled in the same manner as was described in sub-sections 2.1 and 2.2 for the single-loop OEO. The difference between the two configurations is clearly the presence of the couplers in the injection bridge which are used to injection-lock between the oscillating signals of the master-loop and the slave-loop in the DIL-OEO. In this sub-section we describe how the model takes into account the couplers and how it treats the time synchronization between the two oscillating signals.

We denote the loop delays  $\tau_1$  and  $\tau_2$ , when  $\tau_2 \leq \tau_1$ . Following the terminology in [2], we refer to the OEO loop with the longer loop delay,  $\tau_1$ , as the master loop, and to the OEO loop with the shorter loop delay,  $\tau_2$ , as the slave loop. We assume an arbitrary carrier frequency  $f_c$  that is approximately equal to the expected oscillating frequency of the DIL-OEO, and we denote the phasors in the master loop and the slave loop with respect to the carrier frequency as  $a_1(t)$  and  $a_2(t)$ , respectively.

The coupling between the two loops is characterized by four complex coefficients,  $\gamma_{ij}$ ,  $i, j = 1, 2$ :

$$\begin{pmatrix} a'_1(t) \\ a'_2(t) \end{pmatrix} = \begin{pmatrix} \gamma_{11} & \gamma_{12} \\ \gamma_{21} & \gamma_{22} \end{pmatrix} \begin{pmatrix} a_1(t) \\ a_2(t) \end{pmatrix}. \quad (7)$$

where  $a_i(t)$  and  $a'_i(t)$  ( $i = 1, 2$ ) are the amplitudes before and after the coupling in the master loop ( $i = 1$ ) and in the slave loop ( $i = 2$ ), respectively. The forward injection coefficient,  $\Gamma_{12} = |\gamma_{12}|^2$ , represents the relative injected power from the master to the slave loop and the backward injection coefficient,  $\Gamma_{21} = |\gamma_{21}|^2$ , represents the relative injected power from the slave to the master loop. Unidirectional injection corresponds to  $\Gamma_{21} = 0$ .

The evolution in the DIL-OEO was simulated by calculating iteratively the change in the phasors  $a_1(t)$  and  $a_2(t)$  in a round trip in each of the OEO loops. In our model implementation, the phasors  $a_1(t)$  and  $a_2(t)$  were sampled with the same resolution time  $\delta t$ , which is typically 50 nanoseconds and was always chosen so that  $\tau_2/\delta t = N_2$  is an exact integer. In a 40 m loop we typically chose  $N_2 = 4$ . In this case, we find  $\tau_1 = N_1\delta t + \delta\tau_1$ , where  $|\delta\tau_1| < \delta t/2$ . In our simulations, we retained  $N_2$  values of  $a_2(t)$  and  $N_1$  values of  $a_1(t)$  in two separate arrays. The arrays of the phasor in the master loop and in the slave loop before the injection bridge are denoted by  $a_1(i_1)$  and  $a_2(i_2)$ , respectively, such that  $i_1 = 1, \dots, N_1$  and  $i_2 = 1, \dots, N_2$ . The arrays of the phasor in the master loop and in the slave loop after the injection bridge are denoted by  $a'_1(i_1)$  and  $a'_2(i_2)$ , respectively. The phasor elements were calculated in each OEO loop and were coupled when they arrive at the coupler.

The time synchronization in the coupling between the two loops was implemented in the model in the following manner: Let  $k = 1, \dots, M$  be the iteration index and  $M$  be the number of the total accumulated terms in the simulation run in each of the loops, such that  $M = T_{\text{tot}}/\delta t$ , and let us assume that  $\delta\tau_1 = 0$ . We let  $i_1 = \text{mod}(k, N_1) + 1$  and  $i_2 = \text{mod}(k, N_2) + 1$ . Thus, the variables  $i_1$  and  $i_2$  pass cyclically through the values  $i_1 = 1, \dots, N_1$  and  $i_2 = 1, \dots, N_2$ . In each iteration, we used  $a_1(i_1)$  and  $a_2(i_2)$ , for which we calculated the phasors after the injection bridge,  $a'_1(i_1)$  and  $a'_2(i_2)$ , using Eq. (7). When  $i_j = N_j$ ,  $j = 1, 2$ , we used the array of the phasor after the bridge,  $a'_j(i_j)$ , in order to calculate the array of the phasor before the bridge,  $a_j(i_j)$ , for the following round-trip. The evolution of the phasor after the bridge in each loop was calculated by taking into account the response of all the lumped components on the phasor, as well as the additive white noise and the multiplicative flicker noise. The evolution of the phasor array in each loop was calculated in the same manner as in the single-loop OEO model that was described in sub-section 2.1 and in [6].

We modeled the case  $\delta\tau_1 \neq 0$  by adding a constant phase shift of  $\delta\phi_1 = -2\pi f_c \delta\tau_1$  to the phasor array of the master loop after it propagates for a time  $N_1\delta t$  that is approximately equal to the round-trip duration of the master loop. Our model's ability to treat the case  $\delta\tau_1 \neq 0$  allows us to take into account the incommensurability of the two loops, which is always present in practice.

We note that the dual-loop OEO model includes all the dynamical effects that were studied in the single-loop model, such as the cavity mode competition during the OEO start-up and temporal amplitude oscillations. These dynamical effects and others are described in detail for a single-loop OEO in Ref. [6].

### 3. Comparison with experimental results

In this section we compare the theoretical and the experimental results for the phase noise in a single-loop OEO and in the DIL-OEO. Good agreement between the theoretical and the experimental results is achieved for both the single-loop OEO and for the DIL-OEO. The Mach-Zehnder modulator's measured parameters values are:  $V_{\pi,AC} = 5$  V,  $V_{\pi,DC} = 3.15$  V,  $V_B = 2.6$  V, and  $\eta = 0.7$ . We used the specified photodetector responsivity: 0.8 A/W at DC and 0.55 A/W at 10 GHz. The measured optical power  $P_0$  is 17 mW and the impedance at the output of the photodetector was  $R = 50$   $\Omega$ . The first step of the comparison was to compare the theoretical and the measured RF power at the output of the detector. We added an effective loss between  $-0.4$  dB and  $-0.9$  dB to the model in order to match the measured RF power. The photodetector's shot noise power density,  $\rho_{SN}$ , was then determined from the round-trip averaged photodetector's current  $I_{PD}$ . We empirically set the noise factor NF of the RF amplifiers — and hence the thermal noise power density  $\rho_{th} = (NF)k_B T$  — and the flicker noise coefficient  $b_{-1}$ , so that we obtained the best match between theory and experiment, as described in sub-section 3.1.

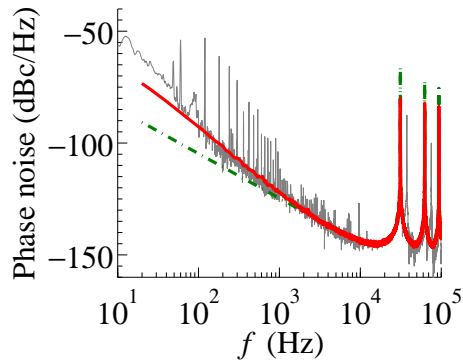


Fig. 4. Comparison between the experimentally measured noise spectral density,  $S_{\text{RF}}(f)$  (solid gray line) and the noise spectral density that is calculated by using a model that excludes flicker noise (dashed-dotted green line) and a generalized model that includes flicker noise (solid red line). All the theoretical curves were calculated assuming the same white noise, oscillation power, and small signal gain. The OEO loop-delay equals  $\tau = 31.7 \mu\text{s}$  and the phase flicker coefficient equals  $b_{-1} = 10^{-11}$ .

### 3.1. Loop length dependance of the phase flicker noise in a single-loop OEO

The coefficient of the phase flicker noise and the noise factor of the RF amplifiers were determined empirically by comparing the theoretical and the experimental phase noise spectra. Figure 4 shows a comparison between theory and experiment in a single-loop OEO with a length of 6400 m, which corresponds to a loop-delay of  $\tau = 31.7 \mu\text{s}$ . The figure shows that in order to obtain good agreement between theory and experiment, a phase flicker noise source must be added. Good agreement between theory and experiment was also obtained when the loop delay was equal to 0.5, 2.7, 7, 10, 15, or 27  $\mu\text{s}$ , corresponding to loop lengths between 100 and 5400 m, when an appropriate amount of flicker noise was added. For all the OEO

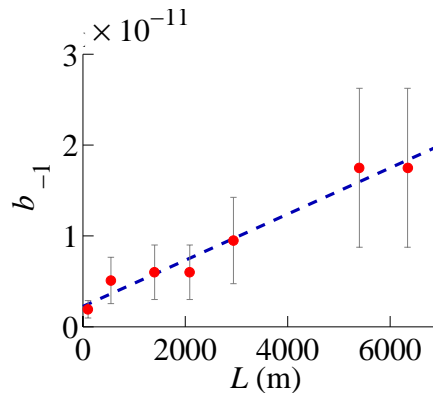


Fig. 5. Dependence of the phase flicker coefficient on the loop length as extracted from single-loop OEO measurements (red dots). The dependence was found to be approximately linear (dashed line):  $b_{-1} = 2 \times 10^{-12} + 2.5 \times 10^{-15}L$ , where the fiber length  $L$  is measured in meters. The accuracy of the extracted dots is limited by the accuracy of the measured data, which is approximately 3 dB. Therefore, the error-bars of the extracted dots are equal to 3 dB.

lengths, the measured oscillation power at the photodiode was  $-22 \pm 1$  dBm and the oscillating power at the output of the RF amplifiers was equal to  $23.3 \pm 0.3$  dBm. The total white noise power density that was used in the theoretical model for all the loop delays was equal to  $\rho_N = 9 \times 10^{-20} \pm 0.5 \times 10^{-20}$  W/Hz, which can be obtained by assuming that the photodetector is limited by shot noise and that the RF amplifiers have a noise factor  $NF = 4$ . The only free parameters in the simulation that we changed when the cavity length was varied were the flicker coefficient  $b_{-1}$ , which determines the power density of the phase flicker noise source, and the effective loss. We varied the effective loss in the model between  $-0.4$  dB and  $-0.9$  dB in order to match the theoretical RF power of the photodetector output to the measured power. We chose the flicker noise coefficient,  $b_{-1}$  so that the theoretical phase noise matches the measured phase noise. Figure 5 demonstrates the dependence of the extracted flicker noise coefficient on the cavity length. Each dot in Fig. 5 was extracted from the measured phase noise. The accuracy of each dot is limited by the noise in the measured data, which approximately equals 3 dB. The figure shows that the flicker coefficient can be divided into a noise component that is independent of the cavity length  $b_{-1} = 2 \times 10^{-12}$  and a component that depends on the cavity length  $L$ . The component that does not depend on the loop length is consistent with the typical flicker noise power that is observed in RF amplifiers [10]. There are several possible sources of the length-dependent flicker noise. These include: conversion of laser frequency noise into phase noise via dispersion and/or laser RIN noise into phase noise via the Kerr nonlinearity, double-scattering processes in the fiber such as double-Rayleigh backscattering or double Brillouin scattering, polarization mode dispersion, and environmental effects. This list is not exhaustive and we intend to study the exact causes of the length-dependent flicker noise in the future. The length-dependent flicker noise is the principal source of phase noise in the low frequency region ( $f < 500$  Hz) of long-cavity OEOs ( $L > 5$  km). The dependence of the flicker noise power on the loop length that was obtained in the single-loop OEO was successfully used as an input to our model for the DIL-OEO.

### 3.2. Comparison between theory and experiment in the DIL-OEO

In this sub-section we present a comparison between the theoretical and the measured phase noise in a DIL-OEO [9]. The experimental setup is described in [7] and a schematic description of the device is given in Fig. 3. A master loop with a length of 4196 m was coupled to a slave loop with a length of 44 m. First, we compared the theoretical and the experimental results for both the slave loop and the master loop in the free-running case when the two loops are not coupled and function as single-loop OEOs. This case corresponds to setting  $\Gamma_{12} = \Gamma_{21} = 0$  and  $\Gamma_{11} = -0.3$  dB,  $\Gamma_{22} = -2.5$ . The other parameters used for the two loops were the same as those we used in the model for the single-loop OEO. We included white noise and flicker noise in the model. The power density of the white noise was equal to  $\rho_{N,1} = 2.4 \times 10^{-20}$  W/Hz for the master loop and to  $\rho_{N,2} = 9 \times 10^{-21}$  W/Hz for the slave loop. The flicker noise coefficient that we used was equal to  $b_{-1} = 10^{-11}$  for the master loop and  $b_{-1} = 10^{-12}$  for the slave loop. The flicker noise coefficient of the slave loop is consistent with the flicker noise coefficient that was measured for RF amplifiers [10]. However, the flicker coefficient in the master loop was considerably higher than in the slave loop, which is in accordance with the results presented in Fig. 5. We obtained excellent quantitative agreement between theory and experiments in the unlocked case, as can be seen in Fig. 6(a).

Figure 6(b) shows the phase noise in the slave and in the master loops when the two loops were coupled and the injection power coefficients were  $\Gamma_{11} = -0.3$  dB,  $\Gamma_{22} = -2.5$  dB, and  $\Gamma_{12} = \Gamma_{21} = -20$  dB. The coupling between the two loops was experimentally implemented using a phase shifter before the coupling bridge in the same loop, so that the coupling coefficients  $\gamma_{ij}$  are real numbers. We obtained good quantitative agreement between theory and

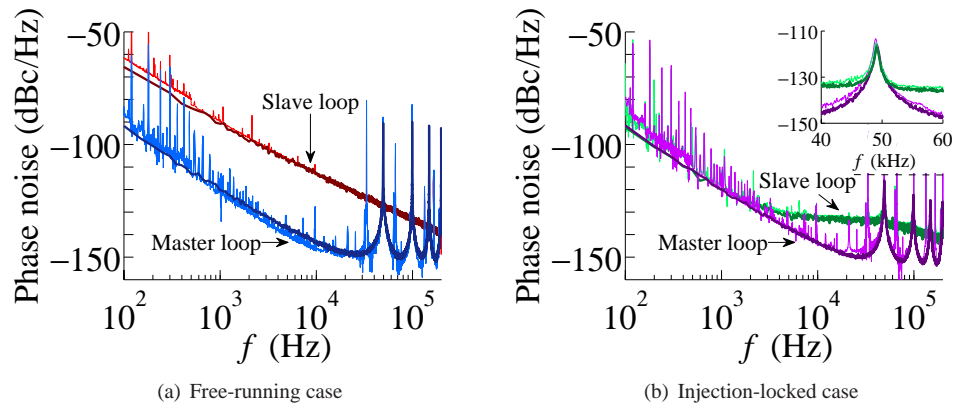


Fig. 6. (a) Phase noise of the master loop (blue) and the slave loop (red) when the loops are free-running and function as single-loop OEOs. (b) Phase noise of the master loop (magenta) and the slave loop (green) when the loops are injection-locked. The inset zooms in on the first spur in the master and slave loops. Good agreement is achieved between the experimental results (thin lines or light colors) and the theoretical results (thick lines or dark colors) when the loops are injection-locked. The injection power coefficients were  $\Gamma_{11} = -0.3$  dB,  $\Gamma_{22} = -2.5$  dB, and  $\Gamma_{12} = \Gamma_{21} = -20$  dB. Theory shows that the first spur in the master loop is about 20 dB lower than in the unlocked case.

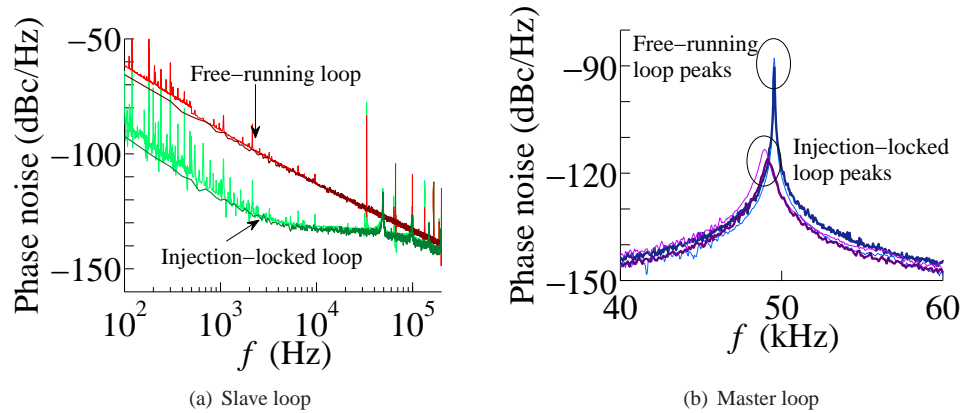


Fig. 7. (a) Calculated phase noise for the free-running slave loop (red) and for the injection-locked slave loop (green) compared to experimental results (thin lines or light colors). The phase noise within the locking range is determined by the master loop. (b) The calculated first spur of the injection-locked master loop (magenta) compared to the spur in the free-running loop (blue). The spur is reduced by approximately 20 dB by injection-locking. The theoretical results (thick lines or dark colors) are also compared to the corresponding experimental results (thin lines or light colors).

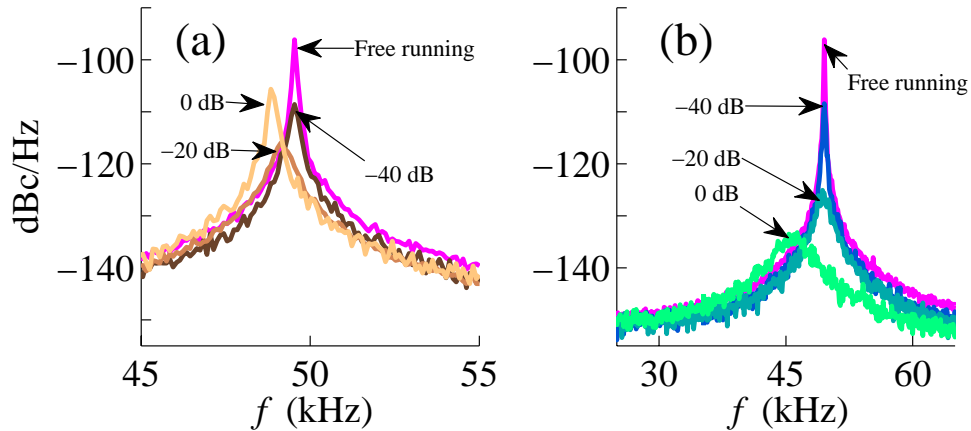


Fig. 8. Calculated spectrum of the phase noise in the neighborhood of the first spur of the master loop as  $R_\Gamma$  varies for  $\tau_1 = 20 \mu\text{s}$  and (a)  $\tau_2 = 0.2 \mu\text{s}$ , (b)  $\tau_2 = 2 \mu\text{s}$ . We show results for  $R_\Gamma = -40$  dB,  $-20$  dB, and  $0$  dB. For comparison, we also show the spur level when the master loop is free-running and functions as a single-loop OEO.

experiment for the phase noise spectrum as well as for the spur levels in both OEO loops in the injection-locked case as demonstrated in Fig. 6(b). Figure 7(a) shows that the model accurately describes the reduction of the phase noise in the slave loop within the frequency locking range of the two loops. Within the locking range, the phase noise in the slave loop is mainly determined by the phase noise of the master loop. Fig. 7(b) shows that the first spur level in the injection-locked master loop is reduced by approximately 20 dB — from  $-95$  dBc/Hz to  $-115$  dBc/Hz — compared to the spur level when it is free-running.

#### 4. Theoretical study of approaches to decrease the first spur in the master loop

In this section, we describe our theoretical optimization of the OEO performance and our experimental verification of the theoretical predictions. A description of the experimental procedures and results is summarized in [8] and will be described in full elsewhere. Our starting point for the theoretical work was the experiments that are described in [7] and in sub-section 3.2. We used the model presented in Sec. 2, and we varied the slave loop length and the power injection ratio, which is defined in the following paragraph. We found a reduction in the first spur by about 20 dB in the injection-locked master loop, relative to the original experiments [7]. These calculations were subsequently verified in experiments.

Our design goal is to reduce the spur level, while approximately maintaining the low phase noise of the free-running master loop. We have chosen to focus on minimizing the phase noise in the master loop rather than in the slave loop since the phase noise of the slave loop is higher outside the locking range.

We have found both theoretically and experimentally that we achieve the best results when  $\Gamma_{12} \simeq \Gamma_{21}$  and  $\Gamma_{11} \simeq \Gamma_{22}$ . We define the power injection ratio  $R_\Gamma = \Gamma_{12}/\Gamma_{11} = \Gamma_{21}/\Gamma_{22}$ , and we will determine the optimum performance as we vary this quantity and the slave loop's delay time. In the computational work that we will present in this section, we have set  $\Gamma_{11} = \Gamma_{22} = 0.25$ . In the experimental verifications that we present here, we set  $\Gamma_{11}$  to within 0.5 dB of  $\Gamma_{22}$ .

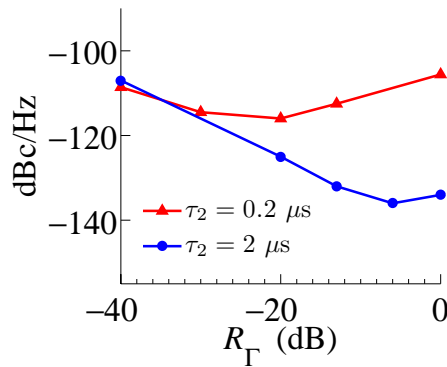


Fig. 9. Calculated dependence of the spur level on the power injection ratio when  $\tau_2 = 0.2 \mu\text{s}$  (red triangles) and when  $\tau_2 = 2 \mu\text{s}$  (blue circles).

Figure 8 shows the calculated noise dependence of the phase noise around the first spur of the master loop as  $R_\Gamma$  varies. In Fig. 8(a), we present results when the slave loop has a loop delay of  $0.2 \mu\text{s}$ , corresponding to a loop length of approximately 40 m, and in Fig. 8(b), we present results when the slave loop has a loop delay of  $2.0 \mu\text{s}$ , corresponding to a loop length of approximately 400 m. We set  $R_\Gamma = -40 \text{ dB}$ ,  $-20 \text{ dB}$ , and  $0 \text{ dB}$ . The other parameters are the same as those that we used for modeling the experimental setup that we described in the previous section. For comparison, we also show the free-running case in both Fig. 8(a) and Fig. 8(b). We recall that when the master loop is free-running, it functions as a single-loop OEO. In Fig. 9, we summarize the key results from Fig. 8 by showing the maximum spur level as a function of  $R_\Gamma$ . We find that the optimal power injection ratio in the original experimental setup [7], in which the slave loop delay is  $0.2 \mu\text{s}$ , is equal to  $-20 \text{ dB}$ . We also find that by increasing the slave loop delay from  $0.2$  to  $2.0 \mu\text{s}$ , the spur level in the master loop is reduced from  $-115 \text{ dBc/Hz}$  to  $-125 \text{ dBc/Hz}$  when  $R_\Gamma = -20 \text{ dB}$  and is further reduced to a level of  $-135 \text{ dBc/Hz}$  by increasing  $R_\Gamma$  to  $-6 \text{ dB}$ . We note that the phase noise of the injection-locked master loop in all the cases that we show in Fig. 9 is approximately equal to the phase noise of the free-running master loop. Thus, we theoretically predict a reduction of the first spur level in the injection-locked master loop by approximately 20 dB relative to the spur level in the original setup, while maintaining approximately the same low phase noise. We note that although Fig. 9 demonstrates the reduction of only the first spur level, other spurs are reduced as well. The second spur level, for example, is reduced from  $-123 \text{ dBc/Hz}$  in the original setup to less than  $-140 \text{ dBc/Hz}$  by increasing the slave loop length from  $0.2 \mu\text{s}$  to  $2 \mu\text{s}$  and by increasing the power injection ratio  $R_\Gamma$  from  $-20 \text{ dB}$  to  $-6 \text{ dB}$ .

The first spur in the master loop can be further suppressed by increasing the slave loop's loop delay beyond  $2.0 \mu\text{s}$ . The level of the first spur in the master loop is mainly determined by the phase noise of the free-running slave loop and the injection parameters. Thus, it is possible to decrease the spur level in the master loop by increasing the length of the slave loop, which decreases the slave loop's free-running phase noise. However, increasing the length of the slave loop reduces its cavity mode spacing and can increase the level of the high-order spurs in the master loop in cases where they nearly coincide with spurs in the slave loop. If these spurs lie within the bandwidth of the RF filter, they can exceed the lower spurs in magnitude and degrade the performance of the DIL-OEO. We have not carried out a detailed study of this issue, as it has not been present in our experiments to date, in which the maximum slave loop delay has been  $2.5 \mu\text{s}$ . However, we note that this issue will place a practical limit on how long it is

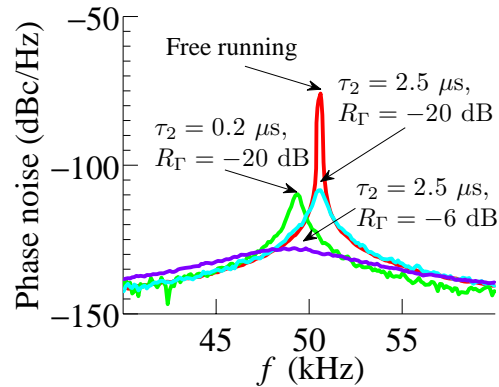


Fig. 10. Experimentally measured spectrum of the phase noise in the vicinity of the first spur. The spur level of the free-running master loop, which has a loop delay of  $\tau_1 = 20 \mu\text{s}$ , was  $-75 \text{ dBc/Hz}$  (red). By injection-locking the master loop to a slave loop with a loop delay of  $\tau_2 = 0.2 \mu\text{s}$  and a power injection ratio of  $R_\Gamma = -20 \text{ dB}$ , we reduced the first spur to  $-110 \text{ dBc/Hz}$  (green). Increasing the slave loop-delay to  $\tau_2 = 2.5 \mu\text{s}$ , and keeping the same power injection ratio, we measured a spur of  $-109 \text{ dBc/Hz}$  (cyan). The spur was reduced to  $-129 \text{ dBc/Hz}$  by increasing the power injection ratio to  $R_\Gamma = -6 \text{ dB}$  (magenta).

possible to make the slave loop

These predictions have been experimentally verified. As noted previously, we predicted optimal results when  $\Gamma_{12} \simeq \Gamma_{21}$  and  $\Gamma_{11} \simeq \Gamma_{22}$  — a point that we experimentally verified. The best spur reduction was achieved by increasing the slave loop-delay from  $0.2 \mu\text{s}$  to  $2.5 \mu\text{s}$  and by varying  $R_\Gamma$ . The loop-delay of  $2.5 \mu\text{s}$  is  $0.5 \mu\text{s}$  longer than in the original theoretical studies. The maximum reduction in the spur level was achieved by increasing  $R_\Gamma$  from  $-20 \text{ dB}$  to  $-6 \text{ dB}$ . To achieve this large power injection ratio, we implemented a new bridge that has  $\Gamma_{11} = -7.5 \text{ dB}$  and  $\Gamma_{22} = -7.0 \text{ dB}$ , so that this bridge has approximately  $6 \text{ dB}$  more loss than in our earlier experiments [7]. We implemented this bridge by using four  $3\text{-dB}$  couplers, with two placed in each loop. In each loop, the front coupler was connected to the rear coupler in each loop and to the rear coupler in the other loop. With this configuration, we could obtain power injection ratios,  $R_\Gamma = \Gamma_{12}/\Gamma_{11} \simeq \Gamma_{21}/\Gamma_{22}$  as large as  $0 \text{ dB}$ . We could then reduce  $R_\Gamma$  by adding attenuators between the front coupler of one loop and the rear coupler of another loop.

We show the experimental results in Fig. 10. The first spur level of the free-running master loop, which has a loop delay of  $20 \mu\text{s}$ , was  $-75 \text{ dBc/Hz}$ . By injection-locking the master loop to a slave loop with  $\tau_2 = 0.2 \mu\text{s}$  and  $R_\Gamma = -20 \text{ dB}$ , the spur level decreased to  $-110 \text{ dBc/Hz}$ . When we increased the slave loop delay to  $\tau_2 = 2.5 \mu\text{s}$  and increased  $R_\Gamma$  to  $-6 \text{ dB}$ , the spur level further decreased to  $-129 \text{ dBc/Hz}$ . These values are both within  $2 \text{ dB}$  of the calculated results with this set of parameters.

However, when we used a slave loop delay of  $\tau_2 = 2.5 \mu\text{s}$  with a power injection ratio  $R_\Gamma = -20 \text{ dB}$  in the experiments, we could not maintain a stable phase lock between the master and the slave loops. The experimentally-measured spur level in this case was  $-109 \text{ dBc/Hz}$ , instead of  $-120 \text{ dBc/Hz}$ , as theoretically predicted. Our model assumes that the master and slave OEO loops are phase-locked, and it will not provide reliable answers unless there is a good lock. These results underline the importance of achieving a good phase lock — not only to achieve good agreement between theory and experiment, but also to obtain good performance from the OEO. We will say more about the conditions to achieve a good phase lock in a future publication.

Increasing the back-injection  $\Gamma_{21}$  from the slave loop to the master loop also reduces the first spur, but at the expense of increasing the master phase noise within the locking range. When the  $Q$  factor of the master loop, as defined in [1], is much higher than the  $Q$  factor of the slave loop,  $Q_1 \gg Q_2$ , the master phase noise in the injection-locked case is approximately unaffected by the locking as long as  $\Gamma_{21} = \Gamma_{12} \ll 1$  [4].

## 5. Conclusions

We have described a comprehensive computational model for studying single-loop and dual-loop OEOs. The model resolves the behavior of the signal during one round-trip in the OEO and takes into account the lumped elements in the loop and both white and flicker noise sources. As a consequence, it allows us to reliably predict the spur level, the effect of large coupling between the two loops in the DIL-OEO, and other dynamical effects. In particular, it can be used to accurately determine the variation of the phase noise in OEOs as their parameters change. An excellent agreement between theory and experiments was obtained for both the single-loop OEO and the DIL-OEO when its two loops are phase-locked.

We used the comparison between theory and experiment in a single-loop OEO to determine the power spectral density of the white noise source and the phase flicker noise source. We found experimentally that the phase flicker noise power spectral density increases linearly with the cavity length. Including this linear dependence in our model was necessary to achieve good agreement between theory and experiment. The increase of the phase flicker noise as a function of the cavity length is important since it limits the performance of long-cavity OEOs. The physical reasons for this dependence have yet to be determined.

We used the free parameters in our single-loop model — the linear loss as a function of length, the power spectral densities of the white noise source and flicker phase noise source as a function of length — in our model of the DIL-OEO. Thus, our model of the DIL-OEO has no additional empirical parameters. The model accurately predicts the phase noise in the master and in the slave loops, the locking range in the slave spectrum, and the spur levels. The model can be used to study a general case of coupling between two OEO loops. In particular, it allows us to reliably study OEO loops that are strongly coupled to each other.

Due to its accuracy and its ability to analyze OEOs with different configurations over a wide parameter range, our computational model can be used to optimize the performance of OEOs. We showed theoretically that it is possible to reduce the first spur in the master loop of the DIL-OEO by about 20 dB relative to our original experiments [7]. This reduction was subsequently verified experimentally [8]. We obtained this reduction by increasing both the loop-delay of the slave loop and by increasing the power injection ratio, so that the two loops are strongly coupled.

## Acknowledgement

This work is supported by DARPA MTO.